



Prediction of Optimum Welding Parameters for Weld-Quality Characterization in Dissimilar Ultrasonic-Welded Al-to-Cu Tabs for Li-ion Batteries

Michael de Leon¹ · Hyung-Seop Shin¹

Received: 27 March 2022 / Accepted: 27 June 2022 / Published online: 8 August 2022
© The Author(s) under exclusive licence to The Korean Institute of Metals and Materials 2022

Abstract

Recently, battery capacity and performance improvements have become the most important issues for improving the performance of electric vehicles. Improvement of the aluminum and copper junctions used as battery tab materials is also required. The dissimilar tab materials are connected either in series or parallel to deliver the required battery power and capacity to the vehicle. Ultrasonic welding is increasing in popularity for joining dissimilar materials, and the automotive industry is likely to benefit the most. However, the industry is dealing with variations in joint quality due to the numerous welding parameters involved, such as the welding time, vibration amplitude, welding pressure, etc. Therefore, in this study, an appropriate design-of-experiment method was used to optimize the selected welding parameters with a reduced number of tests in terms of weld strength quality (either under lap-shear or T-peel tests) and electrical joint resistance. The signal-to-noise ratio and strength-reduction ratio analyses were employed to investigate the influence of different welding parameters for each joint-quality category and to predict the optimum welding parameters within the limits of the parameters studied. The analyses were successful and effective in identifying the most influential welding parameter for each category. The results of analyses and predictions generated were satisfactorily comparable with the validation experiment results.

Keywords Ultrasonic welding · Al–Cu joint · Design-of-experiment · Mechanical joint properties · Electrical joint resistance

1 Introduction

Joints of dissimilar materials are increasingly in demand due to their unique advantages if welded properly, such as appropriate mechanical properties and the possibility of component-weight reduction. However, there are issues related to the compatibility of the materials being joined and the joining process to be employed. According to the study of Anawa and Olabi [1], the differences in the materials' thermal expansion coefficients are associated with thermal residual stresses across the weld area. Post-weld heat treatment is also complicated, especially when the materials being joined have different precipitations at elevated temperatures. Srinivasan [2] added that the electrochemical

property variations in the dissimilar joints can result in problems that are affected by the environment, like cracking, atmospheric corrosion, and pitting.

Ultrasonic welding (UW) is a solid-state joining process that is becoming widely popular for dissimilar joints of metals and alloys, especially when high heat (like in fusion welding) should be avoided. In UW, moderate pressure is applied in combination with localized high-frequency shear vibrations. Since the weld energy can be directly generated at the weld interface, a liquid phase reaction during the welding can be prevented. Progressive shearing and plastic deformation between surface asperities help to soften the weld zone, disperse oxides and contaminants, and expose pure metal contacts, after which the adjacent surfaces bond to each other [3].

For decades, the UW technique has been tried on several types of materials and has overcome many of the metallurgical, environmental, and energy-use limitations of other joining processes. Currently, UW is applicable to materials such as copper (Cu), aluminum (Al), magnesium (Mg),

✉ Hyung-Seop Shin
hsshin@anu.ac.kr

¹ Department of Mechanical Design Engineering, Andong National University, Andong 36729, Republic of Korea

related softer metals such as silver (Ag) and gold (Au), and other highly reflective and conductive materials even in a multi-layered configuration [4]. UW was successfully applied to the joining of thin superconductor tapes, resulting in electrical joint resistances comparable to or lower than those achieved using conventional soldering [5]. UW also proved its effectiveness in challenging environments such as underwater or vacuum environments [6]. Thus, this technique can solve some of the problems of conventional welding in specific applications.

UW has become applicable in a wide range of fields and industries since it was proposed by Daniels [7] for metallic materials. Now, its uses include the fabrication of electrical wire, packaging, medical instruments and electronics, aerospace, and the automotive industry, as have been recently demonstrated [8]. Specifically, the joining of Al and Cu electrodes, tabs, and busbars in lithium-ion (Li-ion) batteries involves several important connections. In fact, joining technology for these connections is considered one of the deciding factors for successful automotive battery systems manufacturing [9]. Problems such as defects, unbonded interfaces, and cracks in these connections could lead to excessive energy loss due to Joule heating [4].

In widely used pouch-type battery modules, several pouch cells are connected, and several modules are arranged in a battery pack. A review on automotive battery pack manufacturing reveals that one of the essential components in the design of a battery for electric vehicles is the cell packaging of the battery unit, where there are numerous tab-to-tab interconnections [10]. However, it is challenging to perform extensive weld-quality characterization and optimization of the weld, including thermal characterization, weld strength analysis for both lap-shear and T-peel joint configurations, and electrical joint resistance, based on experiments alone. One of the reasons might be the complexity and numerous materials, resources, and time needed to determine and optimize the weld qualities, especially when a full factorial design is used to identify all possible combinations for a given set of factors [11]. Several studies that provided insights into these weld quality characterization and optimization of the weld suggested the use of statistical experimental design to optimize the weld input parameters with a reduced number of trials needed [11–14].

The design-of-experiment (DOE) and statistical methods have grown rapidly and have been adapted for many applications in determining and optimizing the weld qualities. The Taguchi method, developed by Dr. Genichi Taguchi, is one of the techniques that use a modified and standardized form of DOE and was found effective in quality engineering applications [15]. The popularity of the Taguchi method is due to its practicality in designing high-quality systems that provide much-reduced variance for experiments with an optimum setting of process welding parameters [16].

The Taguchi method can provide a basis for determining the functional relationship between the controllable factors and the desired outputs and can be used from the experimental design stage to the final optimization process with few experiments needed.

The Taguchi method was used as a systematic and efficient methodology in optimizing the welding parameters using UW and to produce joints that address the concerns involved in tab-to-tab joints. The selection of parameters that significantly influence the weld qualities is important because they affect the quality and strength. A novel and efficient approach is proposed for weld-quality optimization of UW tab-to-tab joints with consideration of multiple performance characteristics.

2 Materials and Methods

2.1 Sample

Commercially available sheets of Al and Cu were used as samples to represent the terminal-tab materials for pouch cell batteries. Tab-to-tab connections were made between 0.2-mm-thick A1050-H16 Al (99.6% purity) and 0.2-mm-thick C1220P-1/2H Cu (99.9% purity). The sheets were cut into coupon-shaped specimens with a length of 100 mm and a width of 20 mm. The thermal properties of Cu are different from those of Al. Cu has a melting point of 1084 °C and thermal conductivity of 340 W m⁻¹ K⁻¹, while those of Al are 660 °C and 230 W m⁻¹ K⁻¹, respectively [17]. However, Al is lighter for the same conductivity, approximately 54% lighter than Cu [18]. Cu is a better option when the space and size of a component are more important than the weight in a specific application. Cu has a 64% smaller cross-section than Al for the same conductivity, which makes it better for reducing volume.

The samples' material properties differ according to tensile tests at room temperature. Cu has an average maximum failure load before fracture of 1330 N, while that of Al is 730 N. Thus, the yield strength (σ_y) and modulus of elasticity (E) of Cu are two times that of Al. The surface hardness values of the two samples are also different (~58 HV for Cu and ~26 HV for Al) based on Vickers hardness tests.

2.2 Ultrasonic Welding Process

Joining was carried out using a lateral-drive UW machine (KORMAX, model KM-2035) in time control mode, and the welding energy and power input were adjusted automatically. Additional details about this welder are available elsewhere [19]. This welder has a single transducer system, so oscillating motion is generated on only the horn side of the overlapped sample to be joined. Nevertheless, it

has the capability of generating up to 3.5 kW of power at a frequency of 20 kHz. Unlike the wedge-reed type ultrasonic welder which utilizes low vibration amplitude and large clamping force, the welding system used in this study uses a small clamping force with large vibration amplitude. Also, accurate measurements of the process parameters at the transducer are possible, including the weld energy/time, clamping force, and vibration amplitude, which makes this welder more suitable for joining thin-gauge sheets.

A horn with a pyramidal tip pattern was used. The vibration direction was applied parallel to the width direction of the lapped sheets. Figure 1a shows the horn and anvil with their respective tips geometries and dimensions. The horn was made of high-speed steel with a rectangular surface shape, which had dimensions of 7 mm × 20 mm. The anvil side (opposing side) length is shorter by 2 mm than the horn side length, so the effective contacting length is only 18 mm. The anvil tips are slightly taller and have a wider base than the horn tips. The tips' patterns were designed according to the dimensions and physical properties of the materials to be welded through the preliminary test selections and in our previous study [20].

2.3 Experimental Procedure and Design of Experiment

Welding was done with a lap-joint configuration, as shown in Fig. 1b, c. Two variations of lap joints were adopted: one for the lap shear test and electrical joint resistance measurement (Fig. 1b) and another for the T-peel test (Fig. 1c). All the lap-joint variant configurations are based on an actual Li-ion battery tab-to-tab welding application, as shown in the battery cell image in Fig. 1.

A lap-joint specimen configuration with proper positioning of the thinner sheet or softer sheet is an important consideration not only in multilayered UW but also in dissimilar Al-to-Cu joints, as previously demonstrated [20].

Therefore, to prevent severe deformation, distortion, and thinning of the Al sheet, it was placed in the lower position of the lap-joint configuration facing the anvil side. Three different levels of welding time, vibration amplitude, and welding pressure were used in this study, as shown in Table 1, while the initial gap between the horn and anvil without the samples was kept at 0 mm.

Taguchi's DOE method was used with three levels of three factors (welding parameters). These factors are controllable parameters that can be adjusted from the welder. Through the Taguchi method, the functional relationship between these factors and the desired outcomes of the process (e.g., joint strength, electrical joint resistance, etc.) can be determined. With the desired outcomes, two objective functions were identified for optimization. This can be done through the use of a loss function to measure the performance characteristics that deviate from the desired target value.

The value of this loss function is transformed into a signal-to-noise (S/N) ratio. Generally, there are three categories to analyze the S/N ratio: "nominal-the-best," "larger-the-better," and "smaller-the-better." Larger-the-better and smaller-the-better were adopted in this study. First, for the weld strength (evaluated through lap shear and T peel tests), the focus was on larger is better (see Eq. 1), and for the electrical joint-resistance measurement, the smaller-the-better was used (see Eq. 2).

Table 1 Welding parameters and corresponding levels

Welding parameter	Level 1	Level 2	Level 3
Welding time (s)	0.4	0.8	1.2
Vibration amplitude (%)	50	70	90
Welding pressure (bar)	4	5	6

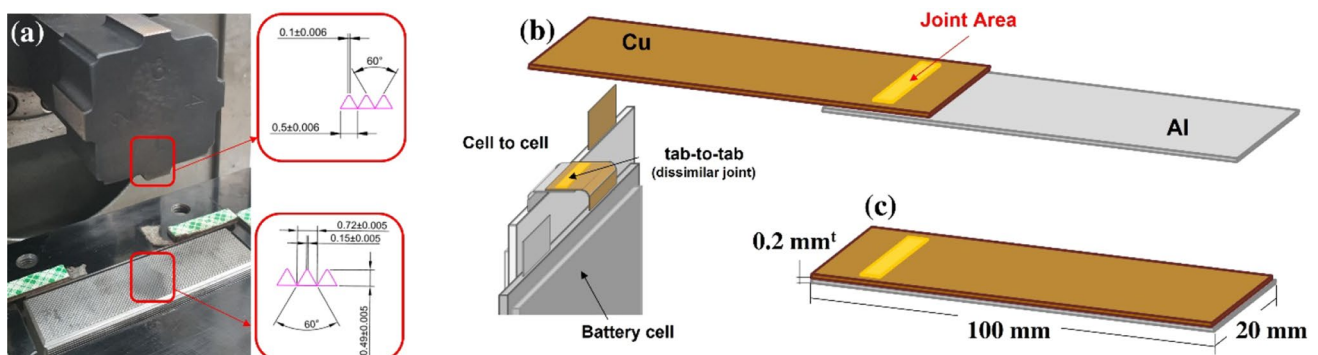


Fig. 1 a Image of the horn and anvil with their corresponding tip patterns and dimensions. Lap-joint specimens for b lap-shear test and electrical joint resistance measurement and c T-peel test. The image in the center represents the battery cell connection

$$\frac{S}{N} = -10 \log \left[\frac{\sum \left(\frac{1}{Y^2} \right)}{n} \right] \quad (1)$$

$$\frac{S}{N} = -10 \log \left[\frac{\sum (Y^2)}{n} \right] \quad (2)$$

Y is the responses for a given factor-level combination, and n is the number of responses in the factor-level combination. The selections of a proper orthogonal array and matrix construction were done using the statistical software Minitab 18 [21]. For parameters with three factors and three levels, an L9 orthogonal array was selected, meaning that nine sets of experiments were conducted.

The matrix constructed for the experimental layout is shown in Table 2. It is composed of three columns (excluding the set number column) and nine rows. Tests for each of the nine rows were conducted three times (27 experiments in total) per performance characteristic to account for the variations that may occur due to other factors. The results of tests of performance characteristics were averaged, and the S/N ratio for each set of parameter combinations was computed.

Statistical analysis was also performed to determine the mean values, standard deviation (SD), and coefficient of variation (COV) to measure the dispersion and frequency of distribution. Most importantly, two-step optimization procedures were done. The first step was the selection of proper control-factor levels to maximize the responses and S/N ratios. This means that the welding parameters and levels with the largest or smallest effect on the desired outcome can be identified. Second, a predicted desired outcome can be defined by adjusting the mean factors to the target values by selecting the level of welding parameters that provides the largest effect on the desired outcome. With the desired outcome identified according to the performance

Table 2 Matrix constructed for the experimental layout from the L9 orthogonal array

Set number	Welding time (s)	Vibration amplitude (%)	Welding pressure (bar)
1	0.4	50	4
2	0.8	70	4
3	1.2	90	4
4	0.4	70	5
5	0.8	90	5
6	1.2	50	5
7	0.4	90	6
8	0.8	50	6
9	1.2	70	6

characteristics, confirmatory tests were conducted using the welding parameters and levels generated by the mean factor adjustment.

The relationship between the T-peel strength and the lap-shear strength was used to provide additional information for selecting the best set of welding parameters based on the joint strength. This method of evaluation is known as the strength reduction ratio (SRR) and can be defined by Eq. 3.

$$SRR = 1 - \frac{\text{T-peelstrength}}{\text{Lap-shearstrength}} \quad (3)$$

This method was recently used by Das et al. [22] in selecting the best joint technology. In the current study, we found that it is also useful when comparing joints welded with different welding parameters using one welding system.

Joints made using the same set of welding parameters were tested in both lap-shear and T-peel loading modes. The concept behind this ratio is that an increase in lap-shear strength should be also observed for T-peel strength in samples welded using the same welding parameters. The higher the SRR, the better the joint quality will be. Typically, joint strengths can be compared by deriving the actual joint strength from the developed nugget size. SRR is independent of nugget size, so it can be used to compare joint strengths without a detailed bonding morphologies inspection.

2.4 Weld Quality Evaluation

The temperature distribution corresponding to the temperature rise was measured using an infrared (IR) thermal imager (FLIR-ThermaCam SC-2000, USA) during the UW process. The goal was to connect the effects of the welding parameters to the weld strength. A lap-shear test was conducted as a mechanical evaluation using a displacement rate of 2 mm/min. For the T-peel test (90° peel test), the joint samples were first bent to a uniform shape using the preparation procedure used in reference [20]. During the T-peel test, a distance of 40 mm between the upper and lower grips was maintained to keep the grip edges from interfering with the deformation of the joint sample during the test.

Next, the peeling force was applied to the specimen at a displacement rate of 20 mm/min, and the peak failure load was obtained. Figure 2a and b show samples that are gripped at both ends before the lap-shear test and T-peel test. Both of these weld strength evaluations were conducted using a universal testing machine with a loadcell capacity of 5 kN (Shimadzu AG-IS).

The four-probe method was used for the measurement of the electrical joint resistance of the UW joint, as shown in Fig. 3. Copper blocks were used to grip specimens at both ends and as current terminals. Two voltage clips made of pure Cu were used with a separation of 20 mm. Worth to

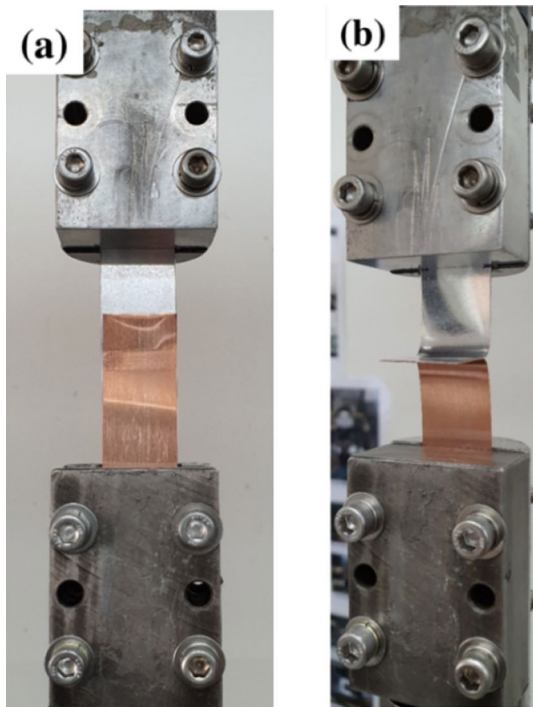


Fig. 2 Lap-jointed samples mounted on a universal testing machine for **a** lap-shear test and **b** T-peel test

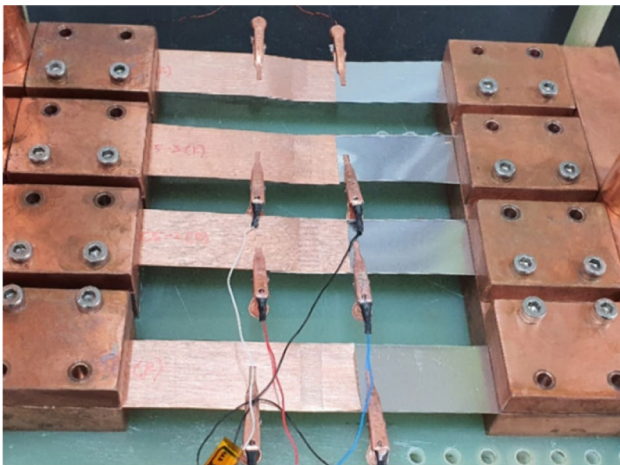


Fig. 3 Electrical joint resistance measurement setup with samples gripped at both ends with current terminals and voltage clips attached between the jointed parts

note that no filler material or solder is used in UW joint. Therefore, aside from the un-jointed sections, electrical joint resistance can be solely derived from any unbonded part or defect at the interface along the joint line. Therefore, it is important to reduce the electrical joint resistance through improving the bonded parts at the interface. The complete details of this measurement using an equivalent electrical circuit are presented in reference [20]. All three evaluations

were used to identify the quality of the weld. The analyses provided by the Taguchi method and relevant statistical analyses from these three evaluations were used to further analyze the results.

The lapped joint surfaces and bonding morphologies were observed using an optical microscope (Olympus SZ60). The lapped welded samples were sectioned across the width axis, parallel to the vibration direction, to characterize the weld quality in terms of weld interface and lapped sheets thinning. Cross-sectioned specimens were first ground by SiC papers up to 2000 grit and further polished by alumina powder up to 0.05 μm .

3 Results and Discussion

3.1 Measurement of Maximum Temperature at the Weld Region

The mismatch of thermal properties could affect the heat generation along a weld interface. As a result, it can have a direct influence on the battery performance by losing the electrical energy across the contact interface and heat generation in the contact area via inhomogeneous thermal expansion [23]. Furthermore, unnecessary and excessive heating of the battery can cause faster battery cell degradation or ageing [24] or even thermal runaway [25], which consequently results in battery cell damage. In extreme cases of heating, even safety issues such as fire or explosions are possible [26]. To observe this, the maximum temperature around the horn tip was measured using an IR thermal imager for each set of welding parameters. A T-type thermocouple was used as a reference to calibrate the IR thermal imager before the maximum temperature measurements. Surfaces with interference sources were shielded (mostly by cardboard) and ambient temperature, air humidity, and camera emissivity adjustments were all performed to guarantee the credibility of the results. Figure 4 shows a representative thermal image captured with temperature distribution at the weld zone. It shows the concentration of heat generated beneath the horn tips while variedly spread along the surrounding area.

The result indicates that significant heat generation occurred due to frictional vibration and plastic deformation and was distributed well over the weld zone. The generated heat is known to be responsible for decreasing the yield strength of materials while generating metallurgical bonding along the weld interface [27]. Patel [28] added that heat generation is also responsible for the plastic deformations at the specimen surface.

Figure 5 shows that the measured maximum temperature in the weld area varied between sets of welding parameters. A maximum temperature of approximately 110 $^{\circ}\text{C}$ was

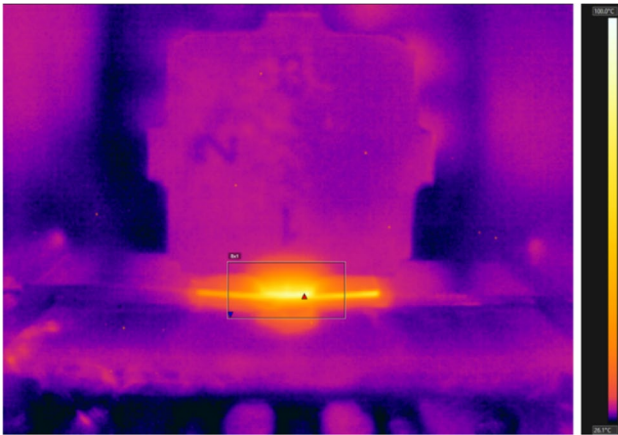


Fig. 4 Infrared image captured at the weld zone with varied temperature distribution along the joint line

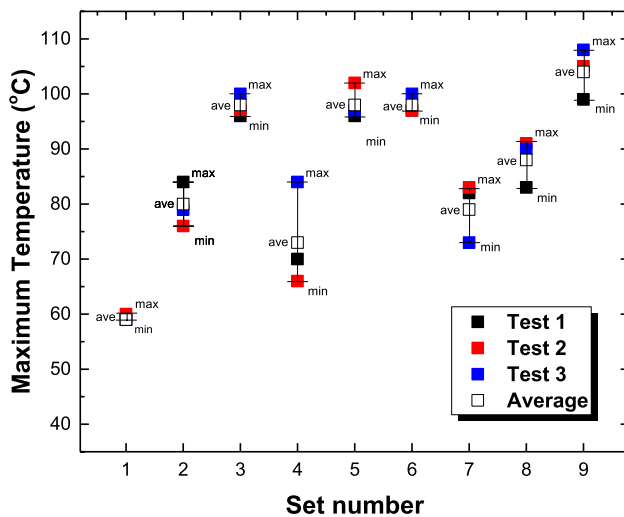


Fig. 5 Results of recorded maximum temperatures in the weld area for each set of welding parameters

observed at the maximum welding pressure and welding time of 6 bar and 1.2 s, respectively. A comparable estimation and extrapolation of weld temperature was obtained in the previous study on a UW joint made for a tab-to-electrode foil with similar material, which had a different thickness and a multilayer configuration and was tested at 0.6 s [20].

With the DOE layout presented in Table 2, the highest maximum temperatures recorded were found to be more sensitive to increasing welding time. Based on the results, the observed temperature rise due to longer welding time is believed to incrementally degrade the weld quality. The maximum temperatures recorded along the weld line were only ~20% and ~10% of the melting points of Al and Cu, respectively. Notably, the temperature range of 60 to 80 °C is critical in a battery cell since the decomposition of

electrochemically active materials in Li-ion batteries starts at temperatures above 80 °C [29]. Temperatures more than that may impair the battery cell capacity and can get intensified if corrosion appears at the weld interface [30]. On a positive note, the location of the measured maximum temperature only concentrates on the center spot of the weld and it was only achieved at the end of the ultrasonic welding process. The temperature dispersed gradually, approximately 10 mm from the center of the weld. This can avoid any possible damage to the sensitive component of the battery if UW processed is utilized in an actual battery joining application. Nevertheless, the electrochemical process in a battery component is temperature dependent, so it is expected that a set of welding parameters that has weld temperatures within the critical temperature range or even less could perform better in terms of the desired weld qualities. For that reason, sets of welding parameters that utilized a welding time of 0.8 s and below, such as sets 1, 2, 4, and 7, might be considered appropriate for generating enough temperature during ultrasonic welding without the problem related to damaging the battery components due to excessive heat.

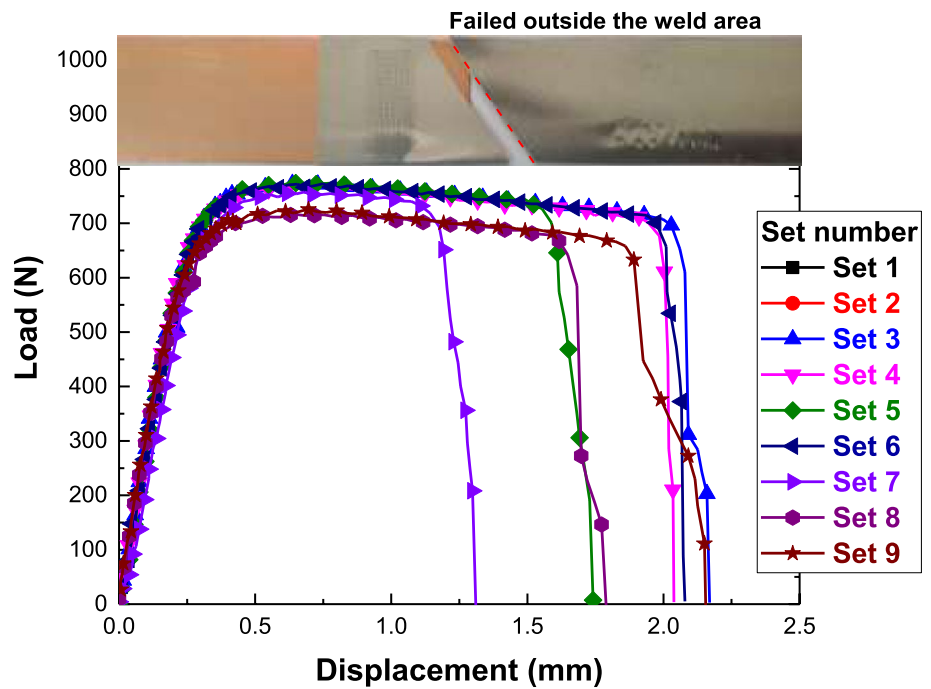
3.2 Lap-shear Strength of Dissimilar Ultrasonic Welding Joints

With Cu and Al, joint fracture could initiate at the weld interface due to the materials' differences in thermal expansions. Figure 6 shows the load–displacement curves obtained from lap-shear tests (only Test 1 results) for all sets of weld parameter combinations. The curves are presented in a line plus scatter plots to easily identify and distinguish the curve for each set. The failure load corresponding to the peak load in each curve varied from 664 to 780 N. Sets 2, 3, and 4 consistently produced higher failure loads (considered here as the weld strength) as shown in Table 3, and larger failure energies (the area under the load–displacement curve, which reflects the weld toughness).

Distinct differences in weld strength and weld toughness between sets 2, 6, and 9 are also noticeable, with set 2 being the best. In addition, scatterings of maximum failure loads are noticeable in sets 6–9. These results are reflected in the weld-part temperature measurements presented in Sect. 3.1, with sets 6 and 9 producing heat generation above the critical temperature range of 60–80 °C.

The inset image in Fig. 6 presents the fracture produced by the lap-shear tests. All fracture results are identical. The failure occurred at the Al sheet outside the weld perimeter, and a crack propagated after the thinning/necking across the width of the sheet at an inclined angle. The average failure load before fracture of a single Al sheet was ~730 N in a tensile test, so it is possible that work hardening of the Al sheet occurred. The failure modes of all lap-shear tests occurred outside the weld area, so it is difficult to directly

Fig. 6 Results of lap-shear tests showing the load–displacement curves of all lap-shear tested samples for Test 1 with a representative image of fracture morphology of dissimilar lap-sheared UW joint of Cu and Al sheets



correlate the weld strength with the observed failure mode. Nevertheless, the heat generated during UW in the weld area and the surrounding areas might influence the variations of failure loads.

Table 3 summarizes the failure loads and the S/N ratios according to the larger-the-better criterion in Eq. 1. The results indicate the influence on the deviations from the average responses (lap-shear strength) of lap-shear tests. Figure 7 shows an evaluation of the responses for each welding parameter and level (i.e., average S/N ratio is equal to 57.79 and 775.2 N for lap-shear strength for all tests at 4-bar welding pressure). Both the calculated ranges ($\Delta = \text{max} - \text{min}$) in the response tables for the lap-shear strengths and the S/N ratios in Fig. 7 consistently show that the welding pressure is the most important factor in the responses. The welding time has the least relevant effect among the factors, meaning

that the lap-shear strength will not change significantly by varying the welding time.

For specific welding parameters, the welding pressure of 4 bar was found to obtain higher lap-shear strength than the samples welded with pressures of 5 and 6 bar for both the lap-shear strength and S/N ratios. The increase in welding pressure led to a reduction in lap-shear strength. Similarly, a welding time of 0.4 s and vibration amplitude of 90% were found to be significant in obtaining high lap-shear strength. In contrast to the welding pressure trend, however, the result is reversed in the case of vibration amplitude: decreasing the vibration amplitude led to a reduction of the lap-shear strength from 764 to 748 N. The analysis shows that the combinations of the welding parameters can be interactive and changeable and are useful to maximize the lap-shear strength and minimize its variation due to noise.

Table 3 Summary of statistical analysis and responses for signal-to-noise ratios for lap-shear strengths

Set #	Test 1 (N)	Test 2 (N)	Test 3 (N)	Lap-shear strength (mean) (N)	Standard deviation (N)	Coeff. of variation (%)	S/N
1	774	759	767	767	7.5	0.98	57.69
2	771	787	778	779	8.0	1.03	57.83
3	779	778	784	780	3.2	0.41	57.85
4	773	776	771	773	2.5	0.33	57.77
5	758	778	742	759	18	2.38	57.60
6	716	764	739	740	24	3.25	57.37
7	726	763	767	752	23	3.01	57.52
8	664	776	767	736	62	8.46	57.27
9	665	777	765	736	62	8.36	57.27

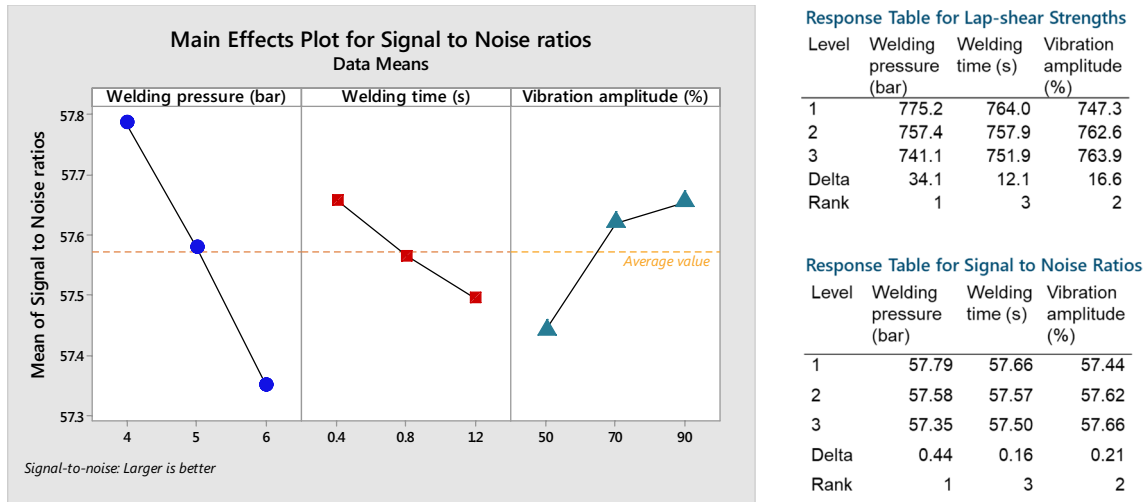


Fig. 7 Main effects plot for signal-to-noise ratios at various levels of factors for lap-shear strength. The tables on the right summarize the responses for lap-shear strengths and signal-to-noise ratios

The next step of predicting the responses was conducted using the optimal levels of welding parameters that significantly affect both the lap-shear strength and S/N ratios. Figure 8 shows that the predicted set result for the mean lap-shear strength value is equal to 787.3 N with a dispersion of 14.8 N. The predicted lap-shear strength is 12 N larger than the highest lap-shear strength obtained by experiments. Similarly, the variation in the predicted response is minimized at an S/N ratio of ~ 58.

The differences between the predicted responses and experimental responses are small. Notably, all lapped sheets failed at the Al alloy sheet, which has an average tensile strength of ~ 730 N. This implies that the lap-shear strengths at the dissimilar Cu-Al UW interface are higher, so they are limited by only the strength of the Al sheet. Nevertheless, the Taguchi analysis and predicted-response results could be valuable for developing optimization models in future work.

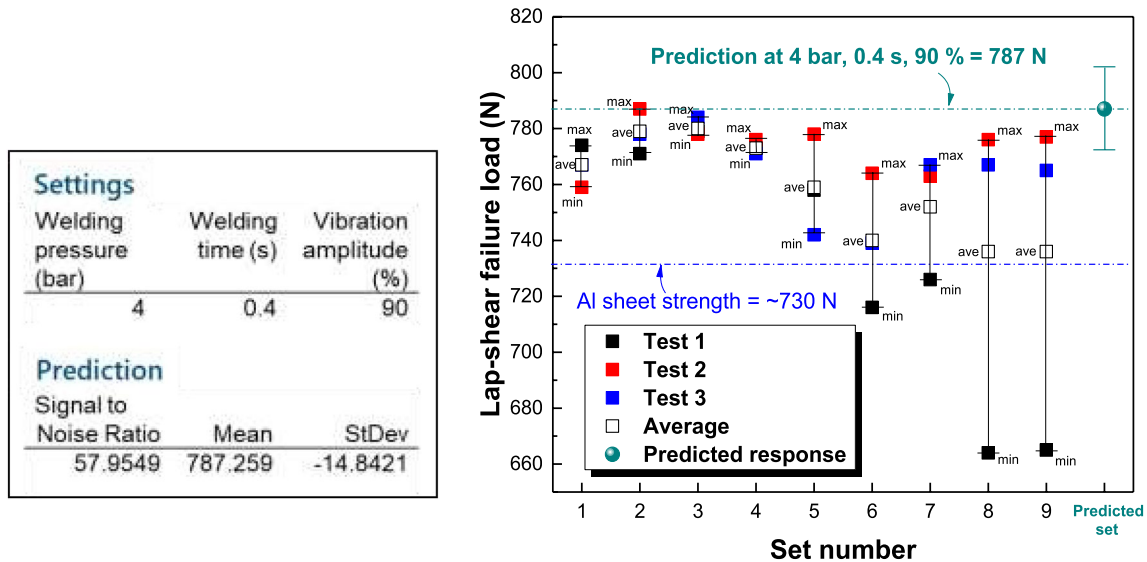


Fig. 8 Plot of the predicted lap-shear strength with standard deviation using the identified optimal welding parameters (welding pressure of 4 bar, welding time of 0.4 s, and vibration amplitude of 90%). The

figure also shows the results of the lap-shear tests showing the maximum lap-shear strengths for all sets of welding parameters and the predicted lap-shear load (predicted set)

3.3 T-peel Strength of Dissimilar Ultrasonic Welding Joints

The T-peel strength is typically lower than the lap-shear strength for almost all kinds of welds. However, joints made with a T-peel configuration are important for certain applications, especially in the automotive sector, where it is desirable to correlate the weld nugget diameter to the weld strength [31]. In this study, nugget development was found after the dominant failure mode of through-thickness tearing occurred outside the weld area and along its perimeter after the T-peel test of dissimilar Cu and Al tab-to-tab lap joints.

Figure 9 shows the load–displacement curves obtained from T-peel tests (only Test 1 results) for all sets of weld parameters combinations. The representative image of the fractured joint showing the tearing of the Al sheet outside and within the weld area perimeter is also presented in

Fig. 9. The highest T-peel strength (maximum load before fracture) reached 189 N, and the lowest value was 100 N. These T-peel strength results are nearly ¼ of the lap-shear strength results presented in Sect. 3.2, and they are quite comparable to those in a recent report [22]. Similar to the lap-shear strength results, it seems that the combinations of welding parameters in set 2 attained the highest T-peel strength.

The larger-the-better criterion for S/N ratios was also used to obtain the optimal welding parameters that are insensitive to noise or variation. Table 4 summarizes the average responses for T-peel strength, S/N ratios, and other statistical measures to check the data dispersions. The two-step optimization procedure by the Taguchi method was again conducted, and Fig. 10 shows the results of the main effects for S/N ratios. Again, the combination of welding parameters that maximizes the T-peel strength (response for means) and

Fig. 9 Results of T-peel tests showing the load–displacement curves of all T-peel-tested samples for Test 1 with a representative image of fracture in dissimilar UW Cu–Al lap-joint by T-peel test

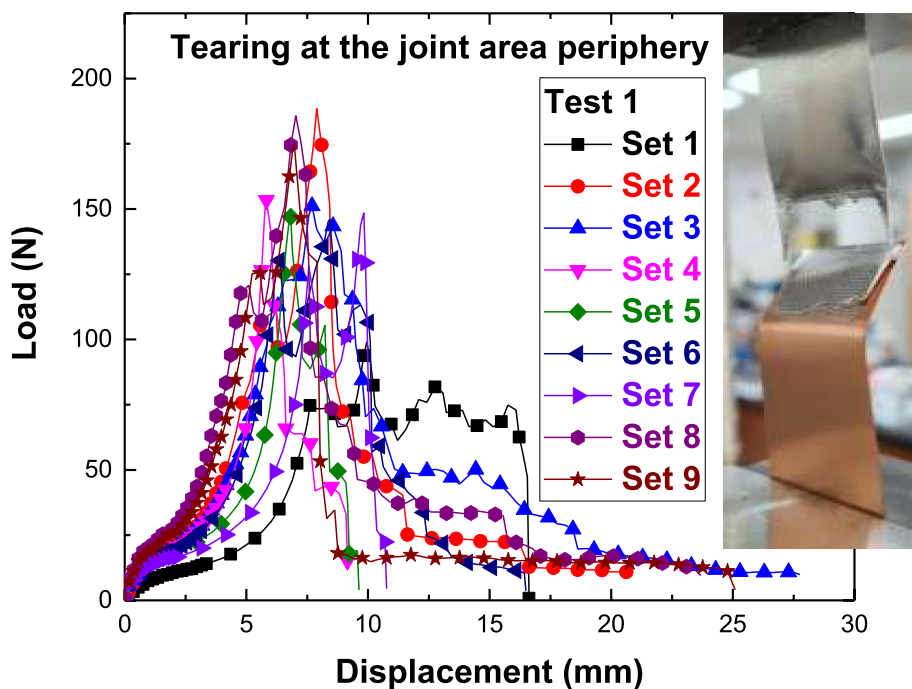


Table 4 Summary of statistical analysis and responses of signal-to-noise ratios for T-peel strengths

Set #	Test 1 (N)	Test 2 (N)	Test 3 (N)	T-peel strength (mean) (N)	Standard deviation (kN)	Coef. of variation (%)	S/N
1	99	76	89	88.0	11.5	13.1	38.74
2	189	186	137	170.7	29.2	17.1	44.35
3	151	148	126	141.7	13.7	9.6	42.94
4	153	121	106	126.7	24.0	19.0	41.76
5	147	132	148	142.3	9.0	6.3	43.03
6	146	156	135	145.7	10.5	7.2	43.22
7	149	143	156	149.3	6.5	4.4	43.47
8	189	126	133	149.3	34.5	23.1	43.08
9	175	144	137	152.0	20.2	13.3	43.50

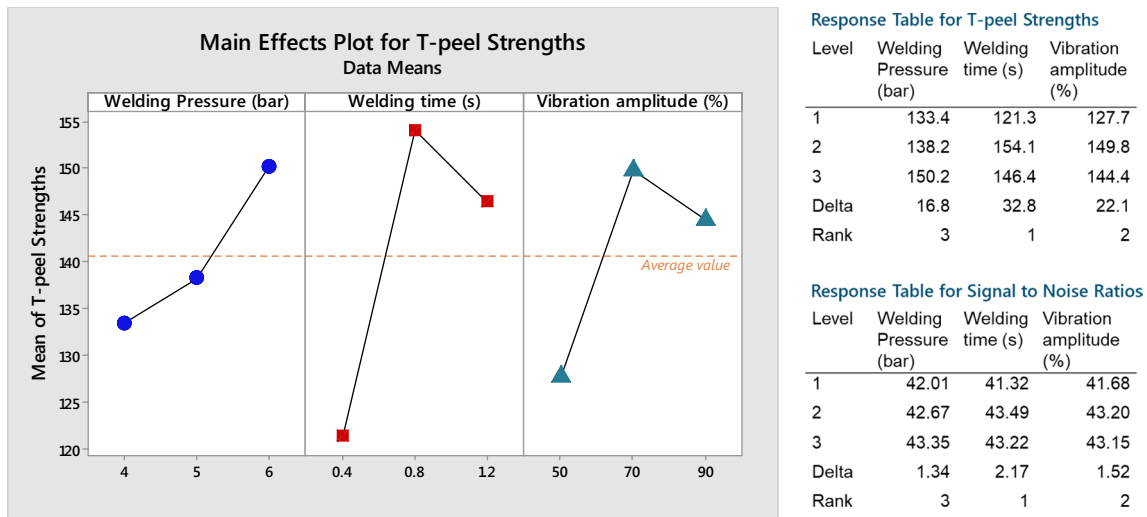


Fig. 10 The main effects plot for T-peel strength at various levels of factors. The tables at the right summarized the responses for T-peel strength and signal to noise ratios

minimizes the variation in the T-peel strength (response for S/N ratios) are identical: a welding pressure of 6 bar (level 3), welding time of 0.8 s (level 2), and vibration amplitude of 70% (level 2).

When decreasing the welding time, the T-peel strength decreases to 121.3 N. For the welding time and vibration amplitude, the highest values of T-peel strength are at level 2. As mentioned earlier, although the welding pressure of 4 bar (level 1) in set 2 achieved the highest T-peel strength,

the mean response for all tests with that welding pressure is lower than the other responses from other welding parameters, as shown by the value of delta = 16.8 in Fig. 10. In fact, the welding pressure was ranked as the least influential factor in the response, while the welding time was ranked as the most influential one in both T-peel strengths and S/N ratios.

Figure 11 shows the results of prediction using the adjusted means of the process by optimizing the controllable

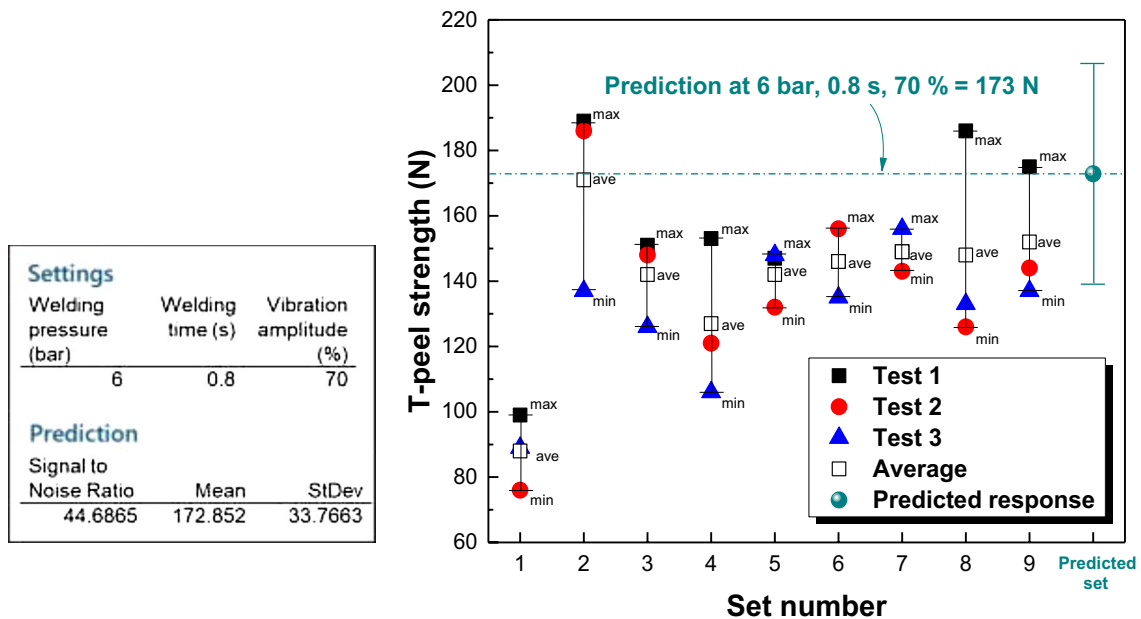


Fig. 11 Plot of predicted T-peel strength with standard deviation using the identified optimal welding parameters (welding pressure of 6 bar, welding time of 0.8 s, and vibration amplitude of 70%). The

figure also shows the results of the T-peel tests showing the maximum T-peel loads for all sets of welding parameters and the predicted maximum T-peel strength (set 10)

variables added to the plot of experimental results for all sets of welding parameter combinations. The predicted set response for the T-peel strength is 173 N and could reach over 200 N when using the optimal welding parameters of a welding pressure of 6 bar, welding time of 0.8 s, and vibration amplitude of 70%. An increase of 19 N from the previous highest T-peel strength of 154 N was obtained. The interactions among the welding parameters in improving the weld quality are complicated and time-consuming, especially with a conventional DOE approach. However, with the Taguchi method, the T-peel strength could be improved with a reduced number of experiments, minimum variation, and consistent weld quality.

3.4 Electrical Joint Resistance of Dissimilar Ultrasonic Welding

It is important to study the Joule heating and electrical imbalance due to poor joints in a battery pack for an electric vehicle. The desired electrical joint resistance should be kept as low as possible to prevent energy loss between the

battery components and to maintain the power capability and efficiency of the battery. This challenging issue has been evaluated recently for electrode foils-to-tab UW joints [20] and for tab-to-busbar joints [32]. Both studies found that a significant correlation exists between the electrical joint resistance and the weld quality, especially with the weld qualities that cannot be explained well by the weld strength and fracture morphologies.

For the dissimilar tab-to-tab UW joints between Cu and Al, a similar approach was used in this study with a four-probe method to evaluate the weld quality and optimize it using the Taguchi method. Figure 12a–c show the measured current–voltage (I–V) curves up to ~10 A current. The electrical resistances of the joints were derived from the slopes of the curves. The lower slopes correspond to the lower electrical joint resistances. For the results, the slopes of sets 6 and 9 have the lowest electrical joint resistances, while sets 1, 2, and 7 have comparable values.

Table 5 shows a summary of the electrical joint resistances for all tests with different welding-parameter combinations. Dispersion of the electrical joint resistances is

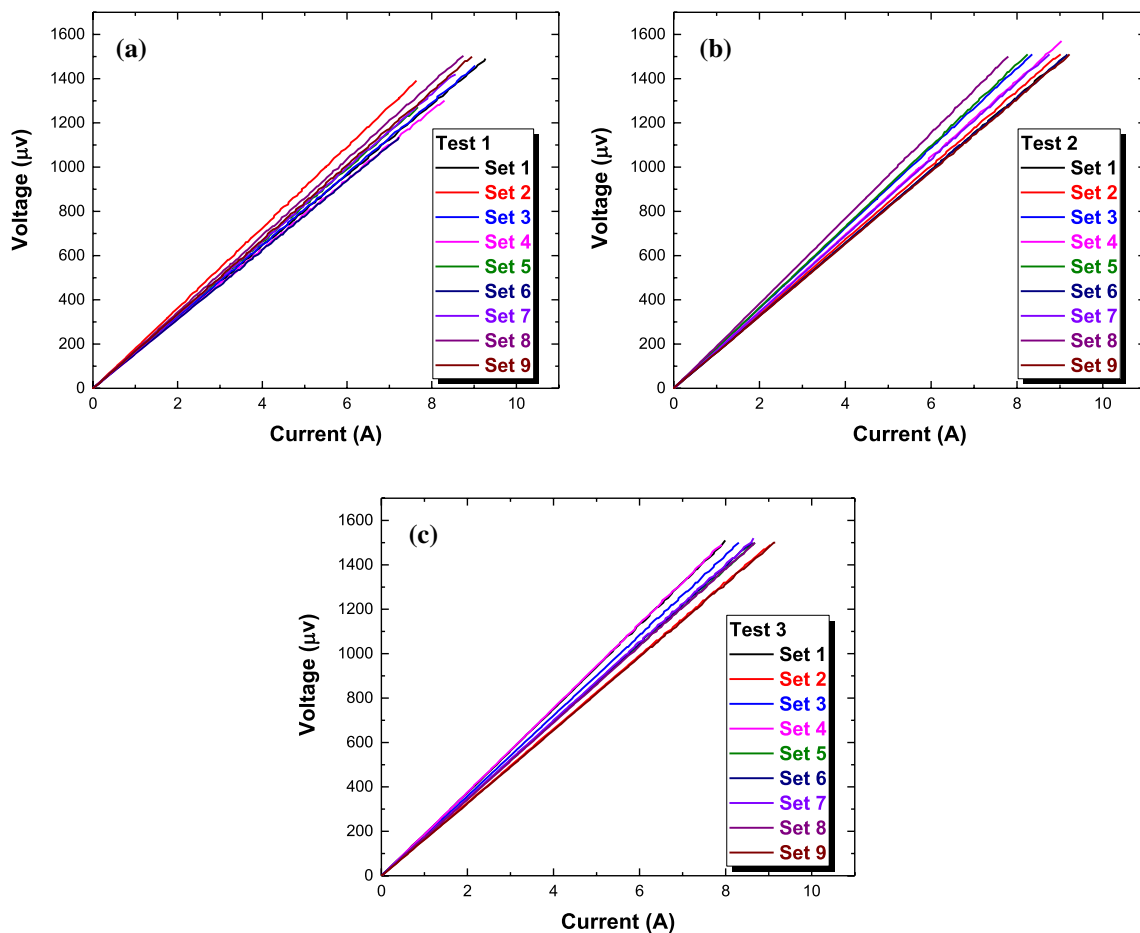


Fig. 12 Results of current–voltage curves of all electrical joint resistance measurements for a Test 1, b Test 2, and c Test 3

Table 5 Summary of statistical analysis for electrical joint resistance and responses for signal-to-noise ratios

Set #	Test 1 ($\mu\Omega$)	Test 2 ($\mu\Omega$)	Test 3 ($\mu\Omega$)	Electrical joint resistance (mean) ($\mu\Omega$)	Standard deviation ($\mu\Omega$)	Coef. of variation (%)	S/N
1	161	165	189	172	15.1	8.82	- 44.71
2	182	168	165	172	9.07	5.29	- 44.71
3	162	181	180	174	10.7	6.13	- 44.81
4	157	174	189	173	16.0	9.24	- 44.81
5	166	183	173	174	8.54	4.91	- 44.81
6	156	165	175	165	9.50	5.75	- 44.41
7	167	173	175	172	4.16	2.43	- 44.71
8	173	193	173	180	11.6	6.43	- 45.11
9	168	164	165	166	2.08	1.26	- 44.41

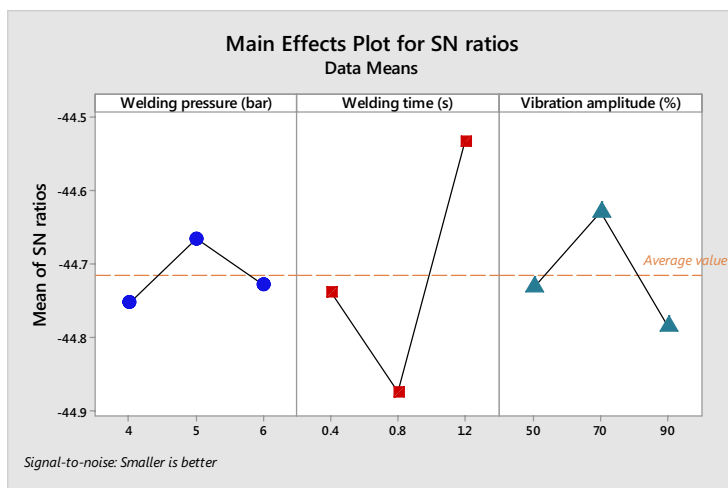
minimal according to the results of standard deviations and coefficient of variations, and the maximum data spreads are only 16 $\mu\Omega$ and 9.24%, respectively. This is considerable since no other joint configurations are used, and the sheet positioning was the same for all tests (only the weld parameters were changed). Nevertheless, it is important to assess the responses to identify the optimal welding parameters, which was conducted using the Taguchi method.

The responses for the electrical joint resistance and S/N ratios in Table 5 are evaluated in Fig. 13 using the smaller-the-better criterion (the S/N ratios are in absolute values). Fortunately, both the responses for the S/N ratios and electrical joint resistance results showed that the welding time has the highest influence on the process, and the welding pressure has the lowest influence, as shown by the delta ranking in the response tables in Fig. 13. The ranking of the welding parameters for both the electrical joint resistance and S/N

ratios are identical to the results evaluated by T-peel tests: welding time is ranked first, followed by the vibration amplitude and welding pressure.

For specific welding parameters, optimized (smaller) electrical joint resistance results can be achieved by the following combinations: a welding pressure of 5 bar (level 2), welding time of 1.2 s (level 3), and vibration amplitude of 70% (level 2). The predicted electrical joint resistance for these welding parameters is presented in Fig. 14 and embedded in all the experimental tests results for the electrical joint resistance. The predicted set electrical joint resistance shows that it can be reduced to as low as ~ 166 $\mu\Omega$ using the optimized welding parameters, which is a great improvement from the experimental results.

With a standard deviation of 8.5 $\mu\Omega$, the electrical joint resistance could be further reduced to ~ 157 $\mu\Omega$. However, this value could not be reduced any further, and the obtained



Response Table for Electrical Joint Resistance

Level	Welding pressure (bar)	Welding time (s)	Vibration amplitude (%)
1	-44.75	-44.74	-44.73
2	-44.67	-44.87	-44.63
3	-44.73	-44.53	-44.78
Delta	0.09	0.34	0.15
Rank	3	1	2

Response Table for Signal to Noise Ratios

Level	Welding pressure (bar)	Welding time (s)	Vibration amplitude (%)
1	-44.75	-44.74	-44.73
2	-44.67	-44.87	-44.63
3	-44.73	-44.53	-44.78
Delta	0.09	0.34	0.15
Rank	3	1	2

Fig. 13 Main effects plot of S/N ratios at various levels of factors for electrical joint resistance. The tables on the right summarize the responses for electrical joint resistance and S/N ratios

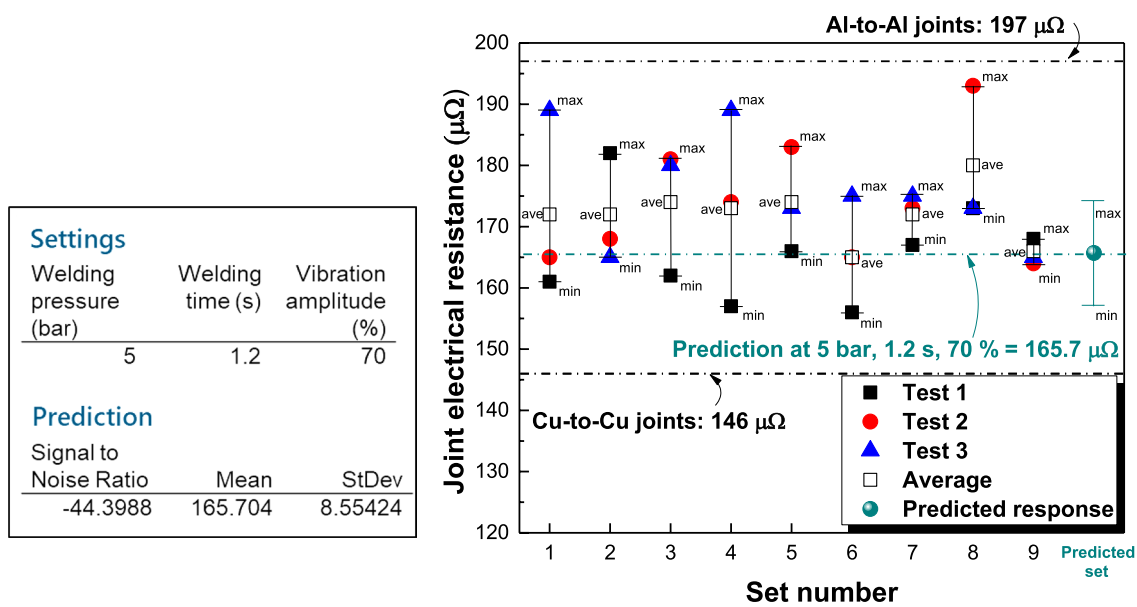


Fig. 14 Predicted values for signal-to-noise ratio and electrical joint resistance with standard deviation using the identified optimal welding parameters (welding pressure of 5 bar, welding time of 1.2 s, and vibration amplitude of 70%). Results of electrical joint resistance for

all sets of welding parameters are summarized in the graph. Electrical joint resistances for similar Cu-to-Cu and Al-to-Al joints are shown with the predicted response for electrical joint resistance

result might be at the lowest threshold of the range. The reason is that a similar Cu-to-Cu UW lap-joint has an electrical joint resistance of 146 $\mu\Omega$. The electrical joint resistance of dissimilar Al and Cu cannot be lower than that. This limiting factor is due to the difference in the intrinsic resistivity between Al (Al: $2.65 \times 10^{-8} \Omega m$) and Cu (Cu: $1.68 \times 10^{-8} \Omega m$) [33]. Figure 14 includes results for similar UW lap-joints Cu to Cu and Al to Al as dotted lines.

The optimal welding parameters were validated using experiments. Five tests were conducted to assess the possible data scattering and to check the consistency of the results. The experimental validation from the tests resulted in electrical joint resistances of 169 $\mu\Omega$, 161 $\mu\Omega$, 171 $\mu\Omega$, 161 $\mu\Omega$, and 169 $\mu\Omega$, respectively. The averaged electrical joint resistance was 166.2 $\mu\Omega$, which is almost identical to the predicted result of 165.7 $\mu\Omega$. Therefore, the optimized welding parameters, their levels, and their interactions were properly chosen.

3.5 Strength Reduction Ratio Analysis

The weld strength quality was also evaluated through SRR analysis. The SRR is defined in Eq. 3 and was used to provide an indication of the difference in strengths of lap shear tested and T-peel tested lapped joints. The process is simple yet powerful enough to identify the possible welding combinations by using only the lap-shear and T-peel strengths without digging into the complex procedure of bonding morphologies and actual nugget-size

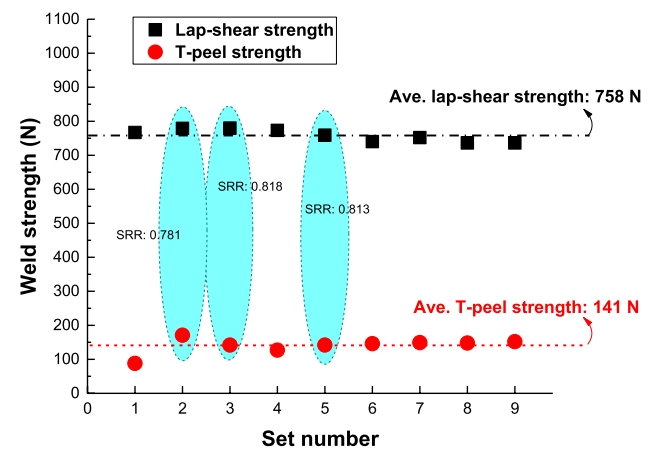


Fig. 15 Weld strength obtained by lap-shear and T-peel tests used to calculate the strength reduction ratio. The strength reduction ratio values for the acceptable sets 2, 3, and 5 are calculated using Eq. 3 and included in the plot

measurement. Figure 15 shows the weld strengths of the lap-sheared and T-peeled samples for all sets of welding-parameter combinations. It shows that the average lap-shear strength is 758 N, while the T-peel strength is 141 N. A criteria for an acceptable SRR value (calculated using Eq. 3) can be set (typically in the range of 0.8 to 1) as a basis for comparison in this study. In cases where a basis for comparison is lacking, the average value of lap-shear and T-peel weld strengths can also be used to calculate a target SRR. Therefore, using the average values of

lap-shear and T-peel tests, the calculated target SRR is 0.814.

In addition, the weld strengths within or above the average value of the lap-shear and T-peel weld strengths were only considered as selected parameters for dissimilar Al-to-Cu UW in this study. Considering the average weld strengths, only welding parameter combinations of sets 2, 3, and 5 satisfied the provided guidelines, so they are selected for further consideration. These three sets are comparatively capable of joining dissimilar Al to Cu with acceptable weld strengths. Among the three selected welding parameter combinations, set 3 has the highest SRR of 0.818 (see Fig. 15). However, the weld strength quality judgment should also consider other factors. Although set 2 has the lowest SRR with respect to calculated target SRR among the three selected sets, its consistency to produce higher weld strengths, both in lap-shear strength and T-peel strength, is commendable, considering that it has the shortest welding time. The generated maximum temperature during the ultrasonic welding should also be considered, in which set 2 generated the lowest one among the three selected sets. The combined lap-shear and T-peel strength for set 2 is higher than sets 3 and 5 (i.e., set 2 = 950 N, set 3 = 922 N, and set 5 = 901 N) while the combined average lap-shear and T-peel strength for all the sets is 899 N. In a case like this, a compromise selection of the optimized set could be made. With set 3 having the highest SRR while set 2 has the highest absolute strength, these two sets could be considered comparable in terms of the joint strength.

Further comparisons between set 2 and other selected sets 1 and 3 are presented in Figs. 16, 17, 18. Surface images

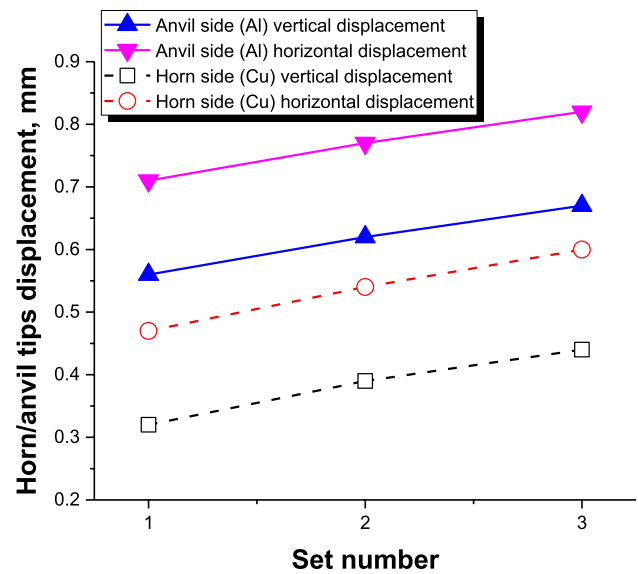


Fig. 17 Horn and anvil tips displacement along the surfaces of the jointed sheets for both Cu and Al. Horizontal displacement represents the direction of the ultrasonic oscillation

with the horn and anvil tips imprints for sets 1, 2, and 3 are presented in Fig. 16a–c, respectively. Tips penetrations on the surfaces are distinct as the welding time and vibration amplitude progress (i.e., from set 1 to set 3). With the Al sheet having a lower hardness value than Cu, tip penetrations are more noticeable with deformations expanded outward by the oscillating vibration. The extents of deformations are clearly seen in the increasing tips penetrations measured in the magnified images in Fig. 16 and in the corresponding

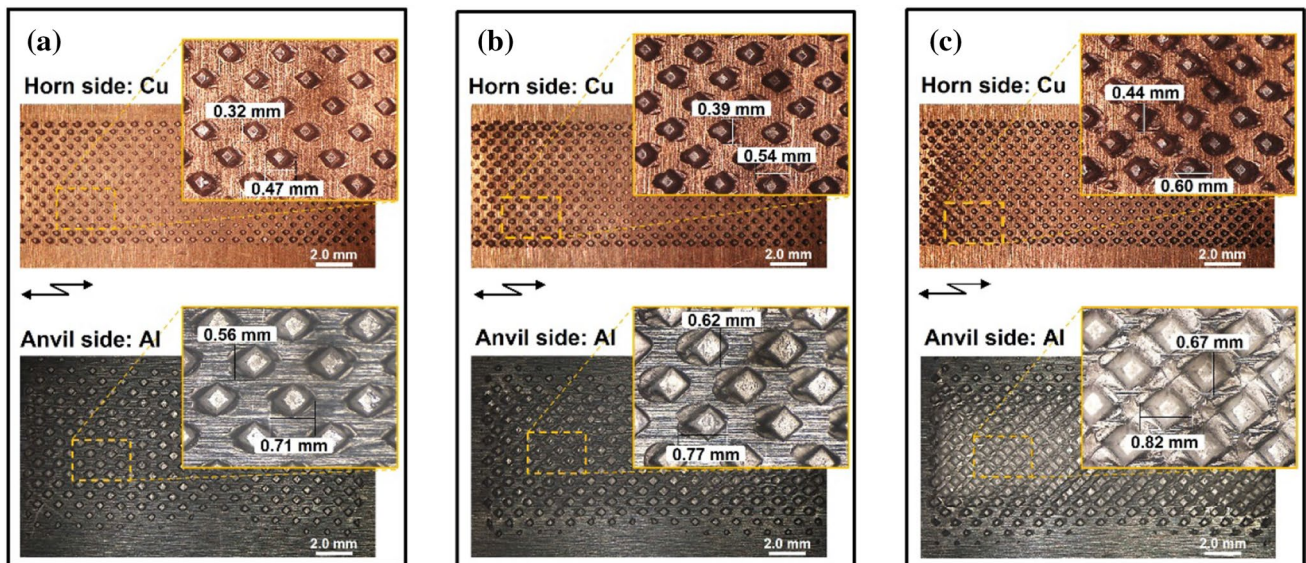
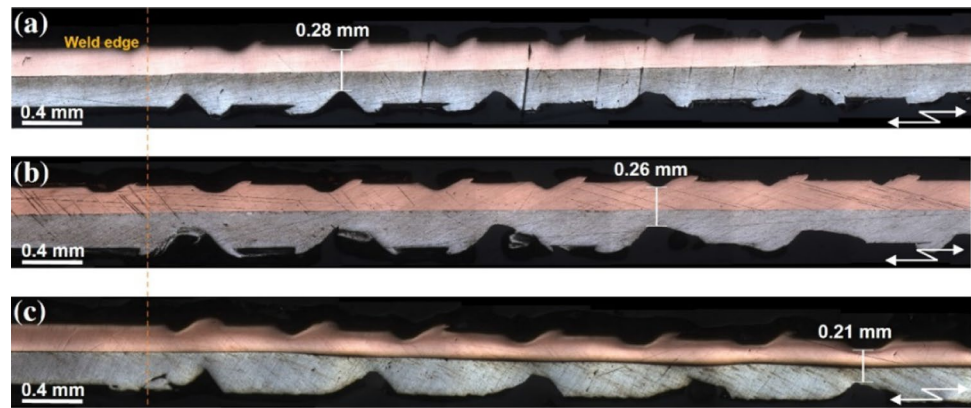


Fig. 16 Surface images with horn/anvil tips imprints taken from the horn side (Cu sheet) and anvil side (Al sheet) of selected sets after ultrasonic welding. **a** Set 1, **b** set 2, and **c** set 3. Vibration direction was applied in the horizontal direction of the images

Fig. 18 Cross-sectional images of jointed samples, showing the horn and anvil tips penetrations and weld zone thinning for **a** set 1, **b** set 2, and **c** set 3. The vibration oscillation direction is parallel to the horizontal direction, as shown in the images



horn and anvil tips displacement plotted in Fig. 17. Almost a linear increase in the tips' imprints can be observed in both Cu and Al sheets as the welding time and vibration amplitude progresses. Although extended tip imprints were observed, no cracking or damage-like defects were observed along the edges and periphery of the joints, suggesting a good weld quality. Post weld examinations of the weld cross-sections in Fig. 18 reveal the impact of the tip imprints on the surfaces of the sheets to the weld zone thinning and the material flow from the tips region to the valley region (the region between tips indentations). For example, in set 3, having the longer welding time and higher vibration amplitude, weld zone thinning was observed noticeably. In the locations where the horn and anvil tips were directly opposed to each other, weld zone thinning was observed to be half of the thickness of one sheet (0.21 mm for set 3). Although no excessive waviness was observed between the lapped interfaces for sets 1 and 2 at the current magnification scale, the tip displacements triggered the material to flow sideways. This sideways flow of materials is most distinct in set 2. On the other hand, interface waviness was observed for set 3. Unfortunately, the excessive lapped sheets thinning deformed the joint line, resulting in scarce locations of unbonded regions. These results further support the reasons why set 2 showed the higher weld strength results among other sets.

The critical welding parameters for weld quality characterization showed that optimal welding-parameter combinations could vary depending on the desired weld quality (e.g., lap-shear strength, T-peel strength, electrical joint resistance, etc.). The Taguchi method successfully identified the optimal welding parameters for each desired weld quality in this study. Although a unified welding parameter combination could be unfeasible for different weld qualities, the methods used here can eliminate the complexity of experiments and evaluations needed to fully analyze the study. The weld quality results for the predicted sets presented in Figs. 8, 11, and 14 could be very useful for the researchers and engineers alike to easily identify the factors

and settings that make the process robust. The identification of the optimum factors and the process of adjusting those factors to minimize the effects of the uncontrollable factors (noise) can be easily performed. The predicted outcomes from the Taguchi method (such as in electrical joint resistances) were also in good agreement with the results of the experiment validations. Further, the results of analyses in judging the optimum welding parameters from only nine sets of welding-parameter combinations were remarkably efficient. A process characteristic map could be developed and a mathematical model, similar to reference [14], could be made from those results.

In instances where there is a conflict between the levels of factors that improve the mean weld strength or electrical joint resistance and those that improve the uniformity of data, a compromise may have to be reached [15]. Fortunately, all analyses of responses for means and S/N ratios consistently ranked the optimal welding parameters. On the other hand, SSR can be very useful in judging the possibility of selecting welding-parameter combinations for further evaluations using the lap-shear and T-peel weld strengths alone. The complexity and time-consuming procedures in observing the nugget size and looking thoroughly at the bonding morphologies could be avoided. In general, the methods and analyses used in this study are essential in determining the critical welding parameters related to UW quality characterization for manufacturing Li-ion battery packs.

4 Conclusion

This paper focused on the critical welding parameters for the weld quality characterization in dissimilar UW Al-to-Cu tabs for a Li-ion battery. The joint weld strengths between Al and Cu combinations were determined from lap-shear and T-peel tests of UW lap-jointed samples, while the electrical joint resistance was obtained from the slope of the current–voltage curve using a four-probe method. The Taguchi

method was used as a DOE method to identify the optimal welding parameters and to predict the equivalent responses for weld strengths (lap shear and T-peel) and electrical joint resistance. The means and signal-to-noise ratios of responses were evaluated according to welding parameters that significantly affect the weld quality. The optimum welding parameter combinations were identified and were found to vary depending on the desired weld quality:

Lap-shear test: Welding pressure of 4 bar welding time of 0.4 s, and vibration amplitude of 90%

T-peel Test: Welding pressure of 6 bar, welding time of 0.8 s, and vibration amplitude of 70%

Electrical joint resistance: Welding pressure of 5 bar, welding time of 1.2 s, and vibration amplitude of 70%

The SRR was assessed and found to be a reliable means of identifying the weld quality based on weld strengths achieved from both lap-shear and T-peel tests with various weld parameter combinations. Furthermore, it could be applied without completely relying on the fracture morphologies and the nugget sizes. Further work could take advantage of this study since the test results and analyses could provide a basis for selecting the optimal welding parameters according to the desired weld quality.

Acknowledgements This research was supported by a grant from the National Research Foundation of Korea (No. 2020-R111A-305839), which is funded by the Ministry of Education (MOE), Republic of Korea.

References

1. E.M. Anawa, A.G. Olabi, *Opt. Laser Technol.* **40**, 379 (2008)
2. P.B. Srinivasan, V. Muthupandi, W. Dietzel, V. Sivan, *Mater. Design* **27**, 182 (2006)
3. G.D. Janaki Ram, C. Robinson, Y. Yang, B.E. Stucker, *Rapid Prototyping J.* **13**, 226 (2007)
4. S.S. Lee, T.H. Kim, S.J. Hu, W.W. Cai, J.A. Abell, in *Proceedings of the ASME 2010 International Manufacturing Science and Engineering Conference*, Erie, 12–15 October 2010. vol. 1, MSEC2010-34168, pp. 541–549
5. M. de Leon, H.-S. Shin, *IEEE T. Appl. Supercon.* **30**, 4600105 (2020)
6. S. Matsuoka, H. Imai, *J. Mater. Process. Tech.* **209**, 954 (2009)
7. H.P.C. Daniels, *Ultrasonics* **3**, 190 (1965)
8. H.-S. Shin, M. de Leon, *Met. Mater. Int.* **23**, 554 (2017)
9. A. Das, D. Li, D. Williams, D. Greenwood, *World Electr. Veh. J.* **9**, 22 (2018)
10. M.F.R. Zwicker, M. Moghadam, W. Zhang, C.V. Nielsen, *J. Adv. Join. Process.* **1**, 100017 (2020)
11. K.Y. Benyounis, A.G. Olabi, *Adv. Eng. Softw.* **39**, 483 (2008)
12. A.R. Singh, C. Sudarsan, A. Das, S. Hazra, S.K. Panda, *J. Mater. Eng. Perform.* **31**, 4133 (2022)
13. S. Elangovan, K. Prakasan, V. Jaiganesh, *Int. J. Adv. Manuf. Tech.* **51**, 163 (2010)
14. J.P. Kumar, *Weld. World.* **64**, 73 (2020)
15. P.J. Ross, *Taguchi Techniques for Quality Engineering* (Tata McGraw-Hill, New Delhi, 2005)
16. N.C. Fei, N.M. Mehat, S. Kamaruddin, *ISRN Ind. Eng.* **2013**, 462174 (2013)
17. MatWeb, <http://www.matweb.com/search/DataSheet.aspx?MatGUID=f54812ceded24176b44c4e0af379ea39&ckck=1>, Accessed 06 January 2022
18. L. Pryor, R. Schlobohm, B. Brownell, *A comparison of aluminium vs. copper as used in electrical equipment* (GE Industrial Solutions, Plainville, USA, 2018)
19. H.-S. Shin, M. de Leon, *J. Mater. Process. Tech.* **224**, 222 (2015)
20. H.-S. Shin, M. de Leon, *J. Mater. Process. Tech.* **241**, 141 (2017)
21. Minitab, <https://support.minitab.com/en-us/minitab/18/help-and-how-to/modeling-statistics/doe/supporting-topics/taguchi-designs/taguchi-designs/>, Accessed 16 December 2021
22. A. Das, D. Li, D. Williams, D. Greenwood, *J. Braz. Soc. Mech. Sci.* **41**, 54 (2019)
23. M. Braunovic, V.V. Konchits, N.K. Myshkin, *Electrical Contacts: Fundamentals, Applications and Technology*, 1st edn. (CRC Press, Boca Raton, 2007), pp. 529–552
24. M. Fleckenstein, O. Bohlen, M.A. Roscher, B. Bäker, *J. Power Sources* **196**, 4769 (2011)
25. N. Yang, X. Zhang, B. Shang, G. Li, *J. Power Sources* **306**, 733 (2016)
26. Q. Wang, P. Ping, X. Zhao, G. Chu, J. Sun, C. Chen, *J. Power Sources* **208**, 210 (2012)
27. M. de Leon, H.-S. Shin, *J. Mater. Process. Tech.* **243**, 1 (2017)
28. V.K. Patel, Ph.D. Dissertation, Ryerson University (2014)
29. M. Brand, S. Glaser, J. Geder, S. Menacher, S. Obpacher, A. Jossen, D. Quinger, in *Proceedings of the 2013 World Electric Vehicle Symposium and Exhibition (EVS27)*. Barcelona, 17–20 November 2013 (IEEE, Piscataway, 2013). <https://doi.org/10.1109/EVS.2013.6914893>
30. C. Campestrini, P. Keil, S.F. Schuster, A. Jossen, *J. Energy Storage* **6**, 142 (2016)
31. A.F. Andreoli, A.M. Chertov, R.G. Maev, *Soldag. Insp.* **21**, 282 (2016)
32. A. Das, A. Barai, I. Masters, D. Williams, *World Electr. Veh. J.* **10**, 55 (2019)
33. Hyperphysics, <http://hyperphysics.phy-astr.gsu.edu/hbase/Tables/rstiv.html>, Accessed 06 January 2022

Publisher's Note Springer Nature remains neutral with regard to jurisdictional claims in published maps and institutional affiliations.

Springer Nature or its licensor holds exclusive rights to this article under a publishing agreement with the author(s) or other rightsholder(s); author self-archiving of the accepted manuscript version of this article is solely governed by the terms of such publishing agreement and applicable law.